RSC Advances

PAPER

View Article Online
View Journal | View Issue

Cite this: *RSC Adv.*, 2017, **7**, 27515

Facile synthesis of Ag_3VO_4/β-$AgVO_3$ nanowires with efficient visible-light photocatalytic activity

Lei Gao,[ab] Zhonghua Li *[b] and Jiawen Liu*[c]

Received 7th April 2017
Accepted 15th May 2017

DOI: 10.1039/c7ra03955g

rsc.li/rsc-advances

Ag_3VO_4/β-$AgVO_3$ nanocomposites were successfully fabricated by chemical precipitation and hydrothermal method. The composites displayed excellent photocatalytic activity in comparision with those of pure β-$AgVO_3$ and Ag_3VO_4, which may be primarily ascribed to the matched energy structures. The sample with a molar ratio of 30% Ag_3VO_4 to β-$AgVO_3$ showed the highest photocatalytic activity for RhB degradation, which was almost 9 and 2.4 times higher than those of pure β-$AgVO_3$ and Ag_3VO_4, respectively. In addition, the trapping experiments also confirmed that holes and hydroxyl radicals are the active species for RhB degradation, and the possible mechanism for enhanced photocatalytic activity was proposed.

1 Introduction

Heterogenerous photocatalysis has gained widespread attention from researchers because it is one of the most green and effective methods to solve the energy shortage and environmental problems.[1–3] Over the past several decades, more and more photocatalysts have been developed, including TiO_2, ZnO, Ta_2O_5 and CuO.[4–10] However, most of them had a high rate of charge carrier recombination and no response in the visible light range. It is very important to effectively utilize solar energy to overcome the above two limitations. Heterostructured photocatalysts,[11–16] an effective media, have been developed to avoid the recombination of photoinduced electron–hole and increase the charge carrier separation efficiency because of the interface electric field. Hence, many different composites have been prepared and reported, such as Ag/AgX,[17] Ag/AgX/GO,[18] RGO/$Bi_{3.64}M_{0.36}O_{6.55}$,[19,20] AgX/$Ag_3PO_4$,[21] $InVO_4$/$BiVO_4$ (ref. 22–26) and $BiPO_4$/Ag_3PO_4.[27]

The monoclinic scheelite Ag_3VO_4 with a band energy of 2.3 eV has received much attention due to its good photocatalytic activity under visible light irradiation. Although the pure Ag_3VO_4 exhibits high photocatalytic performance, its photocatalytic activity is limited because of its low efficiency in separating photogenerated electrons and holes. Hence, many Ag_3VO_4-based heterostructure photocatalysts such as Ag_3VO_4/TiO_2,[28] Ag_2O/Ag_3VO_4/$Ag_4V_2O_7$,[29] Ag_2O/Ag_3VO_4/$AgVO_3$,[30] Ag_3VO_4/Ag_3PO_4 (ref. 31) and Ag_3VO_4/g-C_3N_4,[32] have been developed to enhance the separation of photoinduced charge carriers.

$AgVO_3$ with excellent optical absorption in the visible light region has also attracted considerable attention due to its narrow band gap, high stability and well crystallization.[33–35] However, compared with other Ag-based materials such as Ag_3PO_4,[36] AgX,[37] and Ag_2CO_3,[38] there are only few studies concentrated on degradation of pollutants about $AgVO_3$, which may be attributed to low quantum yield and the poor absorption efficiency in visible light. Therefore, a suitable material coupled with $AgVO_3$ is of great importance to solve its limited application in photocatalysis.

In this study, we reported novel Ag_3VO_4/β-$AgVO_3$ composites through a chemical precipitation approach. We chose one-dimensional β-$AgVO_3$ nanowires as the substrate materials because they have lots of advantages such as visible light responding and supporting materials. A facile chemical precipitation can efficiently suppress the aggregation of Ag_3VO_4 and boost the contact between Ag_3VO_4 and β-$AgVO_3$. The Ag_3VO_4/β-$AgVO_3$ hybrid materials were used for the photodegradation of RhB under visible light and exhibited much higher photocatalytic activity than single Ag_3VO_4 and β-$AgVO_3$. Moreover, a possible photocatalytic mechanism and the stability of the Ag_3VO_4/β-$AgVO_3$ heterojunction were also investigated.

2 Experimental

2.1 Preparation of β-$AgVO_3$ nanowires

All reagents for synthesis and analysis were analytical grade and used without further purification. β-$AgVO_3$ nanowires were synthesized by the previously reported hydrothermal method.[39] 1 mmol NH_4VO_3 (Tianjin bo di reagent co., LTD, Certified China) was dissolved in 60 mL deionized water (Harbin zhong

[a]School of Chemistry and Chemical Engineering, Harbin Institute of Technology, Harbin 150001, P. R. China

[b]Key Laboratory of Microsystems and Microstructures Manufacturing, Ministry of Education, Harbin Institute of Technology, Harbin 150001, P. R. China. E-mail: lizh@hit.edu.cn

[c]Key Laboratory for Photochemical Biomaterials and Energy Storage Materials, College of Chemistry and Chemical Engineering, Harbin Normal University, Harbin 150025, Heilongjiang Province, P. R. China. E-mail: jiawen86@163.com

jia chemical reagent co., LTD, Certified China) with magnetic stirring for 5 min to obtain a transparent solution under room temperature. Then, 1 mmol $AgNO_3$ (Shanghai shi yi chemical reagent co., LTD, Certified China) was slowly added into the above solution and stirred for another 3 min. The pH value of the solution was adjusted to 8–8.2 by using $NH_3 \cdot H_2O$ (25–28%) and then the mixture was homogeneously transferred into five 20 mL Teflon-lined stainless vessel and heated at 180 °C for 12 h. The β-$AgVO_3$ nanowires were collected by centrifugation, washed with deionized water three times, dried at 60 °C for 10 h.

2.2 Synthesis of Ag_3VO_4/β-$AgVO_3$ composites

Ag_3VO_4/β-$AgVO_3$ composites were prepared by a chemical precipitation method. 0.1034 g as-prepared β-$AgVO_3$ nanowires and 0.1010 g $AgNO_3$ (Shanghai shi yi chemical reagent co., LTD, Certified China) dispersed in 40 mL deionized water with magnetic stirring for 5 min. Subsequently, 20 mL of a certain amount of $Na_3VO_4 \cdot 12H_2O$ (Beijing chemical reagent co., LTD, Certified China) aqueous solution was dropped into the above solution and stirred for 3 h. The obtained yellow precipitate was washed with distilled water three times and dried in oven at 60 °C for 6 h. Ag_3VO_4/β-$AgVO_3$ composites with different molar ratios of Ag_3VO_4 were obtained: 5%, 10%, 20%, 30%, 40% and the samples prepared were denoted as 5% Ag_3VO_4/β-$AgVO_3$, 10% Ag_3VO_4/β-$AgVO_3$, 20% Ag_3VO_4/β-$AgVO_3$, 30% Ag_3VO_4/β-$AgVO_3$ and 40% Ag_3VO_4/β-$AgVO_3$, respectively.

2.3 Characterization of Ag_3VO_4/β-$AgVO_3$ composites

The crystalline structures of the samples were recorded on a Rigaku D/MAX-rA XRD (Japan) with Cu K_α radiation (λ = 0.15405 nm) in the range of 20–70° (2θ). The images of the micro-morphology were determined by scanning electron microscopy (SEM, Hitachi, SU8010) and Transmission electron microscope (TEM, Tecnai, G2F30). The surface analysis was studied by X-ray photoelectron spectroscopy (XPS, Thermo Fisher Scientific, ESCALAB250Xi) with a Mg Kα source. The binding energies were calibrated with the C 1s peak of surface adventitious carbon at 284.8 eV. The Ultraviolet-visible Diffuse Reflectance Spectra (UV-vis DRS) were obtained in the range of 255–800 nm using a UV-vis spectrophotometer (UV-2550, Shimadzu, Japan). $BaSO_4$ was used as the reflectance standard material. The BET surface area was measured by N_2 adsorption using a surface analysis instrument (Beishide, 3H-2000PSI, China). The photoluminescence spectra (PL) of the catalysts were recorded using a FluoroMax-4 photoluminescence instrument (HORIBA JobinYvon) with a 350 nm excitation wavelength.

2.4 Evaluation of photocatalytic performance

The photocatalytic properties of the Ag_3VO_4/β-$AgVO_3$ composite samples were evaluated by the degradation of rhodamine B (RhB) dye under visible light irradiation. A 300 W Xe lump was employed as visible light (λ > 400 nm) source and $NaNO_2$ solution was poured between the lump and the photocatalyst to filter out UV light (λ < 400 nm). The vertical distance between the light source and the surface of the solution was about 12 cm. 0.0500 g photocatalyst was dispersed into the 70 mL of RhB (10 mg L^{-1}) in a quartz reactor. Prior to the light illumination, the suspension was stirred in the dark for 30 min to achieve the adsorption–desorption equilibrium on the surface of photocatalyst. At defined time (10 min), about 3 mL of the reaction solution was withdrawn and centrifuged (11 000 rpm, 1 min) to remove the photocatalyst particles. The residual amount of RhB in the solution was recorded by measuring its characteristic optical absorption at 554 nm using UV-vis spectrophotometer.

3 Results and discussion

The typical XRD patterns for the pure β-$AgVO_3$, Ag_3VO_4 and Ag_3VO_4/β-$AgVO_3$ composites are shown in Fig. 1. The pure β-$AgVO_3$ patterns match well with the JCPDS (29-1154) standard data, which suggests that the prepared β-$AgVO_3$ has a monoclinic structure.[40] The diffraction peaks of Ag_3VO_4 can be indexed as the JCPDS (43-0542) standard data.[41] It was clearly found that all the Ag_3VO_4/β-$AgVO_3$ composites exhibit a cooccurrence of both β-$AgVO_3$ and Ag_3VO_4 phases. Furthermore, with the Ag_3VO_4 amounts increasing, the diffraction peak intensity of Ag_3VO_4 becomes stronger gradually. Meanwhile, the diffraction peak positions of β-$AgVO_3$ do not shift, indicating that the introduction of Ag_3VO_4 does not influence the crystal structure of β-$AgVO_3$.

Fig. 2(a) shows the UV-vis diffuse reflectance spectra of pure β-$AgVO_3$, Ag_3VO_4 and Ag_3VO_4/β-$AgVO_3$ composite photocatalysts in order to investigate the optical absorption properties. As depicted from Fig. 2(a), β-$AgVO_3$ and Ag_3VO_4 display excellent optical absorption in visible light. Their absorption edges were approximately 640 nm and 615 nm respectively. From the formula: $\alpha h\nu = A(h\nu - E_g)^{n/2}$, where α is the absorption coefficient, $h\nu$ is the energy, A is a constant, and E_g is the band gap. The value of n depends on whether the transition is direct ($n = 1$) or indirect ($n = 4$) discrete photon in a semiconductor. As shown in Fig. 2(b), we can get the band gap E_g of pure β-$AgVO_3$ and Ag_3VO_4 to be 2.20 eV and 2.37 eV, respectively. Moreover, the potential of conduction band of Ag_3VO_4 and β-

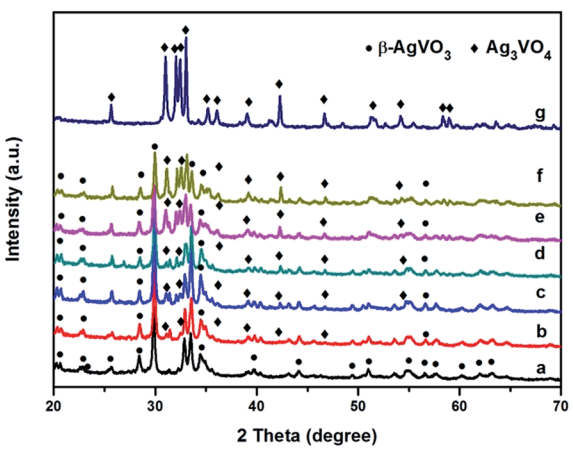

Fig. 1 XRD patterns of β-$AgVO_3$ nanoribbons (a), 5% Ag_3VO_4/β-$AgVO_3$ (b), 10% Ag_3VO_4/β-$AgVO_3$ (c), 20% Ag_3VO_4/β-$AgVO_3$ (d), 30% Ag_3VO_4/β-$AgVO_3$ (e), 40% Ag_3VO_4/β-$AgVO_3$ (f) and Ag_3VO_4 (g).

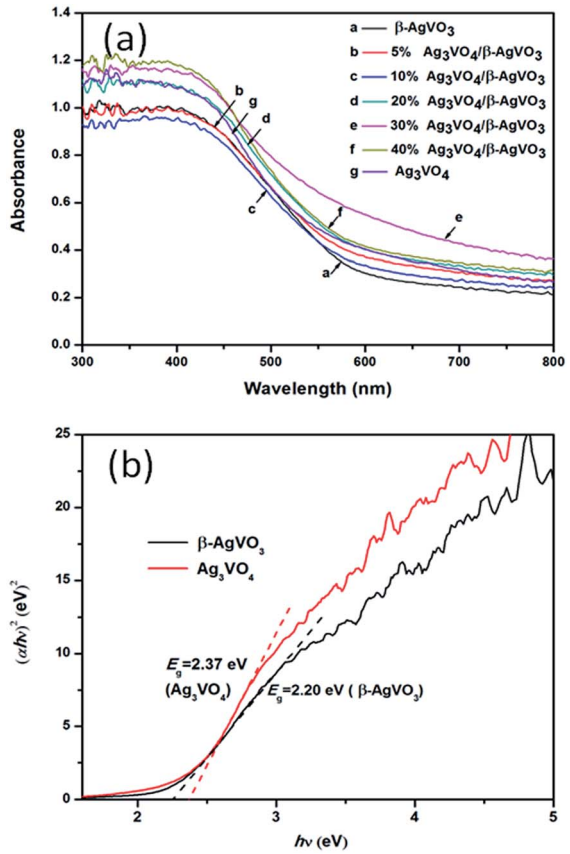

Fig. 2 (a) UV-vis diffuse reflectance spectra of β-$AgVO_3$, Ag_3VO_4 and Ag_3VO_4/β-$AgVO_3$ composites. (b) Plots of $(\alpha h\nu)^2$ *versus* $h\nu$ of pure β-$AgVO_3$, Ag_3VO_4 and Ag_3VO_4/β-$AgVO_3$ composites.

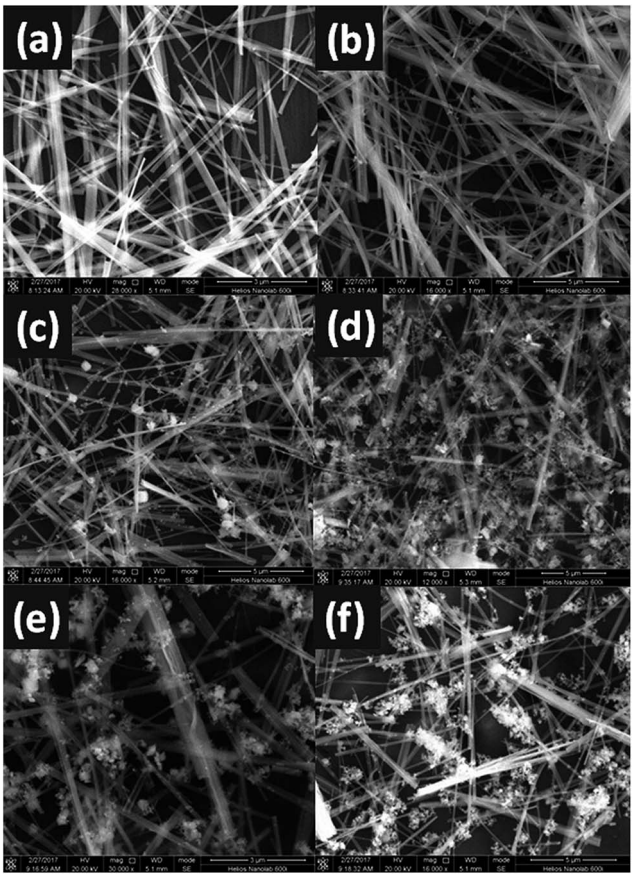

Fig. 3 SEM images of β-$AgVO_3$ nanoribbons (a), 5% Ag_3VO_4/β-$AgVO_3$ (b), 10% Ag_3VO_4/β-$AgVO_3$ (c), 20% Ag_3VO_4/β-$AgVO_3$ (d), 30% Ag_3VO_4/β-$AgVO_3$ (e) and 40% Ag_3VO_4/β-$AgVO_3$ (f).

$AgVO_3$ could be calculated by the following Mulliken electronegativity theory: $E_{CB} = \chi - E^e - 0.5E_g$, where χ is the absolute electronegativity of the semiconductor, E^e is the energy of free electrons (4.5 eV), and E_g is the band gap energy of semiconductor. The χ values of Ag_3VO_4 and β-$AgVO_3$ are 5.64 and 5.88, respectively. So the CB values of Ag_3VO_4 and β-$AgVO_3$ were calculated to be −0.045 and 0.28 eV, respectively. Based on the equation $E_{VB} = E_{CB} + E_g$, the corresponding E_{VB} values were also predicted to be 2.325 and 2.48 eV, respectively. The results indicate that the composite could successfully fabricate the matched energy structures between Ag_3VO_4 and β-$AgVO_3$.

The microstructures of pure β-$AgVO_3$, Ag_3VO_4 and Ag_3VO_4/β-$AgVO_3$ composite photocatalysts were measured by SEM. As shown in Fig. 3(a), pure β-$AgVO_3$ displays a number of nanowires with about 100 nm in width and more than 20 μm in length and its surface is very smooth. As depicted in Fig. 3(b)–(f), the composites of Ag_3VO_4/β-$AgVO_3$ do not influence the shape of β-$AgVO_3$ and the size of Ag_3VO_4 particles becomes larger with the Ag_3VO_4 content increasing, which is in agreement with the enhanced intensity of Ag_3VO_4 XRD patterns.

The morphology of 30% Ag_3VO_4/β-$AgVO_3$ composite is further illustrated by TEM and HRTEM. Fig. 4(a)–(c) show that some Ag_3VO_4 nanoparticles appeared on the smooth surface of β-$AgVO_3$ nanowires.[42] HRTEM in Fig. 4(d) is the location of the circle in Fig. 4(c). By measuring the lattice fringes, the interplanar spacing is 0.317 nm and 0.243 nm, which are corresponding to the (−301) plane of β-$AgVO_3$ and the (202) plane of Ag_3VO_4.

XPS analysis was carried out to further clarify the surface chemical composition and bonding environment of 30%

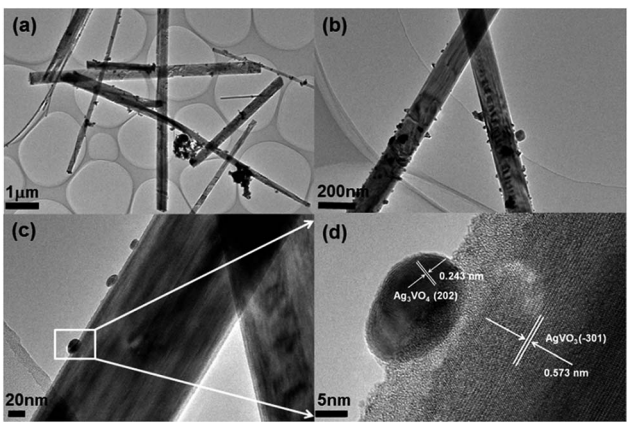

Fig. 4 (a)–(c) TEM images of 30% Ag_3VO_4/β-$AgVO_3$ composite and (d) HRTEM images of the designated square area in panel of (c).

Ag_3VO_4/β-$AgVO_3$ composite and the results are displayed in Fig. 5. The binding energy at 248.8 eV of C 1s is calibrated. The Fig. 5(a) and (b) demonstrates the predominant presence of silver and vanadium. The two peaks at 367.5 and 373.5 eV can be corresponding to the Ag $3d_{5/2}$ and Ag $3d_{3/2}$ of Ag^+ both in Ag_3VO_4 and β-$AgVO_3$.[41,43] The V 2p peaks of 30% Ag_3VO_4/β-$AgVO_3$ at 516.9 and 524.2 eV can be assigned to V $2p_{5/2}$ and V $2p_{3/2}$ of V^{5+} both in Ag_3VO_4 and β-$AgVO_3$.[41,43]

The photocatalytic performance of pure β-$AgVO_3$, Ag_3VO_4 and Ag_3VO_4/$AgVO_3$ composites was evaluated by photocatalytic degradation of RhB under visible light illumination. Fig. 6 displays the experimental results. It can be seen that after 60 min of visible light irradiation the degradation efficiency of pure β-$AgVO_3$ and Ag_3VO_4 were 23% and 57% respectively. Obviously, all the composites have more effective photocatalytic performance than the pure samples, which can be attributed to the presence of Ag_3VO_4 on the surface of β-$AgVO_3$, accelerating the separation of photoinduced electrons and holes. The best photocatalytic performance comes from 30% Ag_3VO_4/β-$AgVO_3$ composite, which is 9 times and 2.4 times than pure β-$AgVO_3$ and Ag_3VO_4. However, with the content of Ag_3VO_4 enhanced to 40%, the decomposition efficiency of RhB declines, suggesting that the excessive Ag_3VO_4 particles deposited on the surface of β-$AgVO_3$ might intervene the photocatalytic activity sites.

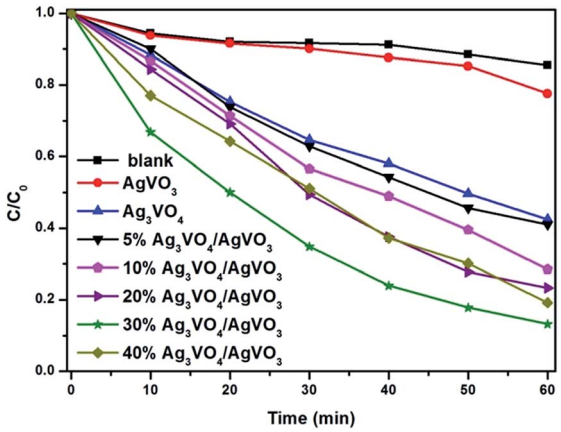

Fig. 6 Photocatalytic degradation of RhB over Ag_3VO_4/β-$AgVO_3$ nanowire composites under visible light irradiation.

Fig. 7 exhibits the obvious changes of RhB solution in UV-visible absorption spectra of 30% Ag_3VO_4/β-$AgVO_3$ composite at different times. It can be clearly observed that the absorbance maximum peak of RhB shifts from 554 nm to 504 nm, which is in good accordance with the previous reports of the degradation of RhB over TiO_2 (ref. 44) and Ag_2O/Ag_3VO_4/$Ag_4V_2O_7$.[29] The color of RhB solution changes from pink to almost colourless after 60 min illumination, which indicates the cleavage of conjugated chromophore structure of RhB.

As depicted from Fig. 8, the experimental results were fitted to pseudo-first-order and all Ag_3VO_4/β-$AgVO_3$ composites exhibit higher photocatalytic performance than single Ag_3VO_4 and β-$AgVO_3$ nanowires. The apparent rate constant k was shown in inset. It can be seen that the composite with mole ratios of 30% Ag_3VO_4/β-$AgVO_3$ shows the highest value of apparent rate constant k, which was 9 and 2.4 times higher than pure β-$AgVO_3$ and Ag_3VO_4. This indicates that the composite

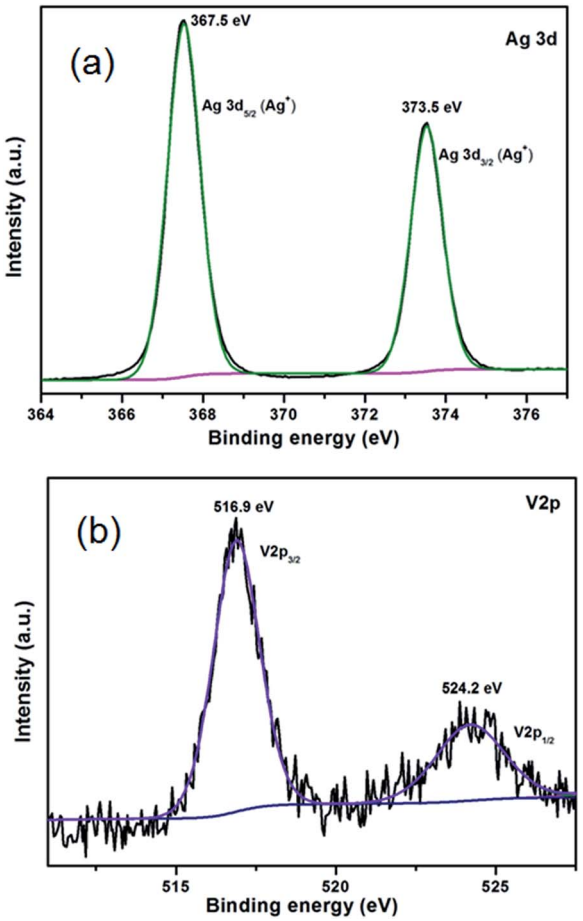

Fig. 5 XPS spectra of 30% Ag_3VO_4/β-$AgVO_3$ composite (a) Ag 3d spectra, (b) V 2p spectra.

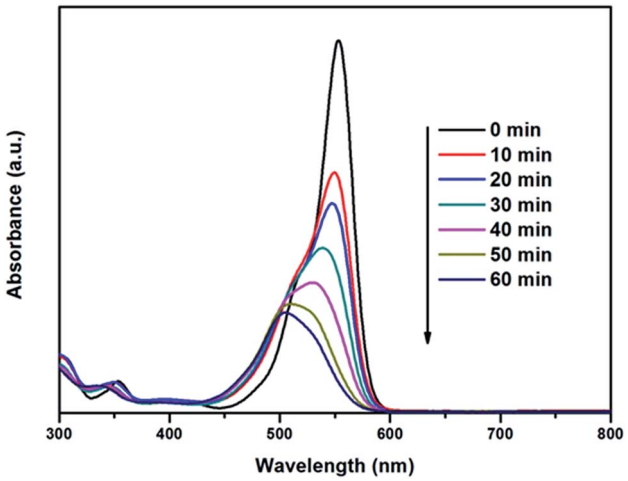

Fig. 7 Changes in UV-visible absorption spectra of 30% Ag_3VO_4/β-$AgVO_3$ photocatalyst at different times under visible light irradiation.

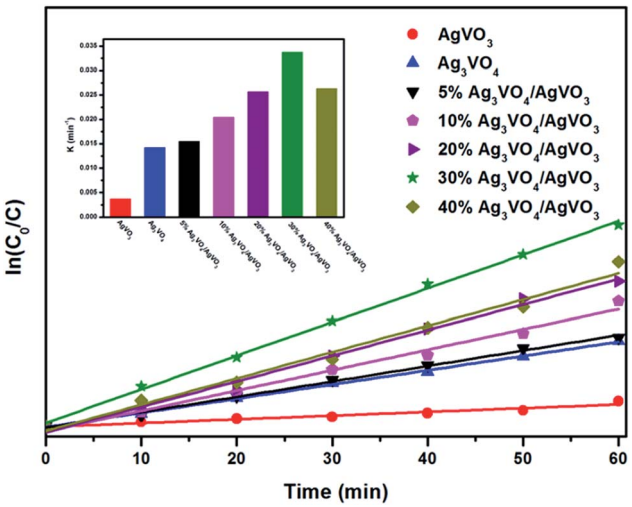

Fig. 8 First-order kinetics of the photodegradation of RhB over β-$AgVO_3$, Ag_3VO_4, and Ag_3VO_4/β-$AgVO_3$ samples under visible light illumination. The inset is the rate constant *k* of the photodegradation of RhB over β-$AgVO_3$, Ag_3VO_4, and Ag_3VO_4/β-$AgVO_3$ samples.

with 30% molar ratio is the most suitable for β-$AgVO_3$ and Ag_3VO_4, which could boost the separation of charge carriers and enhance the photocatalytic performance.

Furthermore, as is shown in Fig. 9, 30% Ag_3VO_4/β-$AgVO_3$ composite has weak adsorption and desorption. The surface areas of β-$AgVO_3$ and 30% Ag_3VO_4/β-$AgVO_3$ composite were 3.096 and 4.610 $m^2\ g^{-1}$, respectively. It was worthwhile to note that the surface area of 30% Ag_3VO_4/β-$AgVO_3$ composite becomes larger with the Ag_3VO_4 nanoparticles deposited on the β-$AgVO_3$ nanoribbons, which can provide more active sites and enhance photocatalytic activity.

The stability of photocatalysts is an important factor for the further application. As is shown in Fig. 10, the photocatalytic activity of the 30% Ag_3VO_4/β-$AgVO_3$ composite still reached 67%, even though it had been used 3 times.

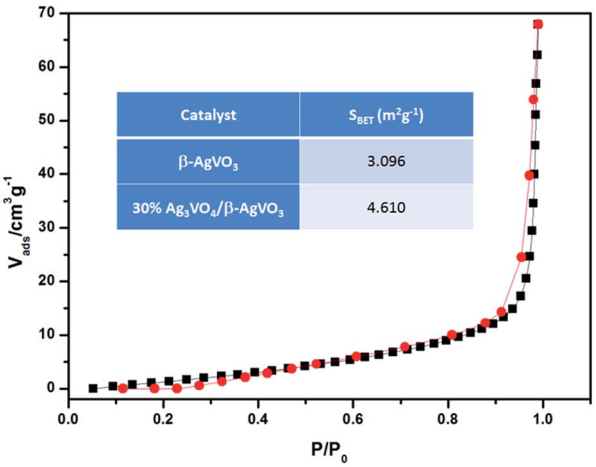

Fig. 9 N_2 adsorption–desorption isotherm of 30% Ag_3VO_4/β-$AgVO_3$ photocatalyst at 393.15 K and the surface areas inset of β-$AgVO_3$ and 30% Ag_3VO_4/β-$AgVO_3$ composite.

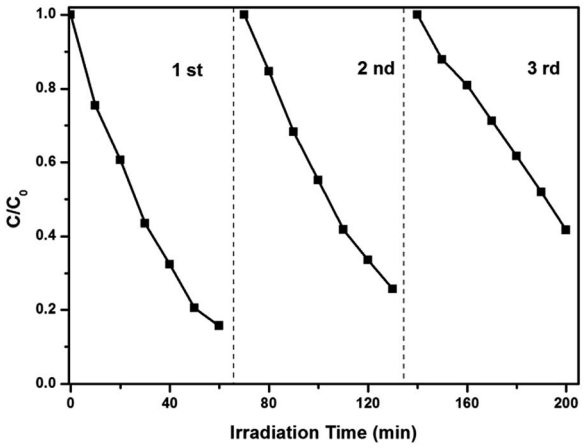

Fig. 10 Cycling runs in the photocatalytic degradation of RhB for the 30% Ag_3VO_4/β-$AgVO_3$.

Additionally, to further reveal the photocatalytic mechanism, the trapping experiments were performed, as shown in Fig. 11. Under visible illumination the photodegradation of RhB is slightly inhibited by adding the IPA (hydroxyl radical scavenger) and ammonium oxalate (hole scavenger), which indicates that hydroxyl radical and hole are the main species that can degenerate RhB.

In order to investigate the process of charge carriers trapping, migration and separation efficiency, the PL spectra of β-$AgVO_3$, Ag_3VO_4, and 30% Ag_3VO_4/β-$AgVO_3$ samples under the excitation wavelength of 350 nm, as shown in Fig. 12. It was generally acknowledged that the lower PL intensity indicates that the higher separation capacity of charge carriers, which results in higher photocatalytic activity. It was observed that the main emission peak of β-$AgVO_3$, Ag_3VO_4, and Ag_3VO_4/β-$AgVO_3$ composites all center at about 595 nm. Compared with pure β-$AgVO_3$ and Ag_3VO_4 samples, the lower PL peak intensity of 30% Ag_3VO_4/β-$AgVO_3$ composites implies that the interface between Ag_3VO_4 and β-$AgVO_3$ can migrates the photogenerate electrons and holes more effectively.

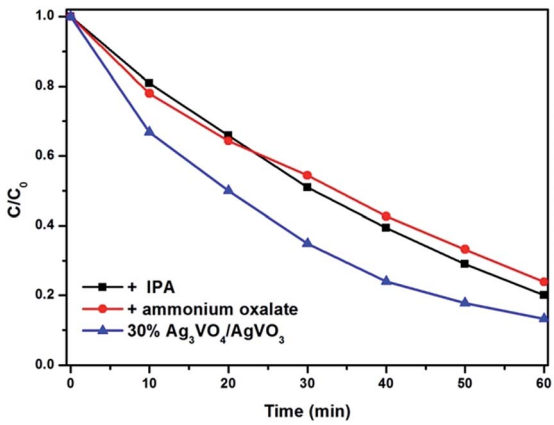

Fig. 11 The plots of photogenerated carrier trapping in the system of photodegradation of RhB under visible light irradiation.

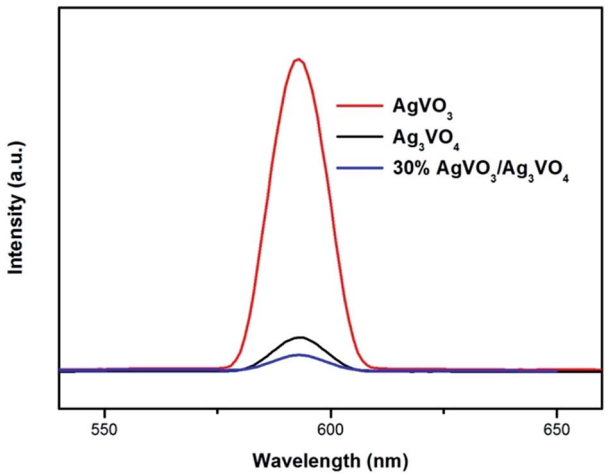

Fig. 12 Photoluminescence (PL) spectra of β-$AgVO_3$, Ag_3VO_4, and 30% Ag_3VO_4/β-$AgVO_3$ samples under the excitation wavelength of 350 nm.

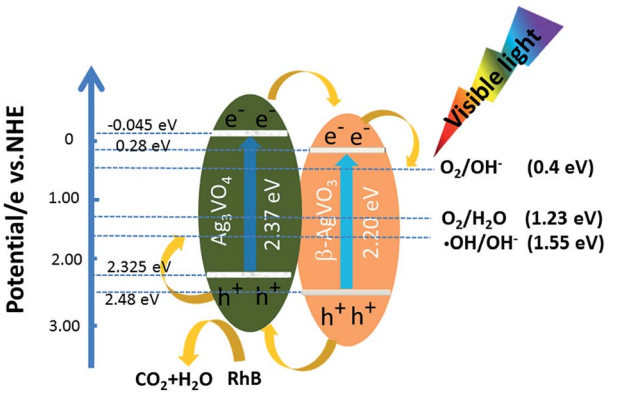

Scheme 1 Photocatalytic mechanism of 30% Ag_3VO_4/β-$AgVO_3$ toward the degradation of RhB.

In fact, the pathway of RhB degradation over Ag_3VO_4/β-$AgVO_3$ composite under visible light is rather complex. Based on the above experimental results and photocatalytic degradation reports, the possible reactions are summarized by eqn (1)–(4).

$$Ag_3VO_4 + h\nu \rightarrow Ag_3VO_4\ (e_{CB}^- + h_{VB}^+) \quad (1a)$$

$$\beta\text{-}AgVO_3 + h\nu \rightarrow \beta\text{-}AgVO_3\ (e_{CB}^- + h_{VB}^+) \quad (1b)$$

$$Ag^+ \text{ (in } \beta\text{-}AgVO_3) + e_{CB}^- \rightarrow Ag^{45} \quad (2a)$$

$$Ag + h\nu \rightarrow Ag\ (SPR) \quad (2b)$$

$$4h_{VB}^+ + 2H_2O \rightarrow 4H^+ + O_2 \quad (3a)$$

$$4h_{VB}^+ + 2OH^- \rightarrow 2H^+ + O_2 \quad (3b)$$

$$h_{VB}^+ + H_2O \rightarrow {}^{\cdot}OH + H^{+30} \quad (3c)$$

$$RhB_{ads} + h\nu \rightarrow RhB_{ads}^* \quad (4a)$$

$$RhB_{ads}^* + e_{CB}^- \rightarrow RhB_{ads}^+ \quad (4b)$$

$$RhB_{ads}^+ + {}^{\cdot}OH \rightarrow N\text{-ethyl rhodamine} \rightarrow CO_2 + H_2O^{46} \quad (4c)$$

In accordance with eqn (1)–(4) and the Scheme 1, the possible mechanism of migration of carriers in the Ag_3VO_4/β-$AgVO_3$ composite heterostructures was discussed. Both Ag_3VO_4 and β-$AgVO_3$ can be excited under visible light illumination according to the UV-vis diffuse reflectance spectra (eqn (1a) and (1b)). The electrons on the conduction band of Ag_3VO_4 can transfer into the conduction band of β-$AgVO_3$ and the holes on the valence band of Ag_3VO_4 can transfer into the valence band of β-$AgVO_3$, because the conduction band of Ag_3VO_4 is negative than β-$AgVO_3$ and the valence band of Ag_3VO_4 is positive than β-$AgVO_3$.[47–50] So, photoinduced electrons and holes can separate effectively, which is crucial for enhancing photocatalytic activities.

After the photoreaction on the Ag_3VO_4/β-$AgVO_3$ composite photocatalyst, the photogenerated electrons of VB transferred to the CB of β-$AgVO_3$ could reduce the Ag^+ to Ag^0 nanoparticles[45] (eqn (2a) and (2b)). However, Ag^0 nanoparticles with SPR in the visible light region could disrupt the ordered transfer of electrons and holes of Ag_3VO_4/β-$AgVO_3$ composite, which results in the gradual declining of photocatalytic activity over Ag_3VO_4/β-$AgVO_3$ hybrid. This is in agreement with decreased photocatalytic performance after three cycling runs.

In addition, the VB potential of Ag_3VO_4 (2.325 eV *vs.* NHE) and β-$AgVO_3$ (2.48 eV *vs.* NHE) were more positive than the standard reduction potential of O_2/OH^- (0.4 eV *vs.* NHE) (3a), O_2/H_2O (1.23 eV *vs.* NHE) (3b) and $^{\cdot}OH/OH^-$ (1.55 eV *vs.* NHE) (3c). Therefore, holes on the VB of both Ag_3VO_4 and β-$AgVO_3$ could react with H_2O and OH^- to form $^{\cdot}OH$, H^+ and O_2, according to eqn (3a)–(3c). Thus, holes and $^{\cdot}OH$ radicals play important roles in the photocatalytic degradation of RhB, which is in good agreement with the experimental result of trapping experiment. Furthermore, the redox potential of RhB (−1.09 eV *vs.* NHE) is more negative than the CB potential of Ag_3VO_4 (−0.045 eV *vs.* NHE) resulting in the self-sensitized degradation of RhB according to eqn (4a)–(4c).

4 Conclusions

In summary, we have successfully synthesized Ag_3VO_4/β-$AgVO_3$ heterojunctions *via* chemical precipitation and hydrothermal method. They show much better photocatalytic activity than pure Ag_3VO_4 and β-$AgVO_3$ toward RhB degradation under visible light and the 30% Ag_3VO_4/β-$AgVO_3$ composite exhibits the highest. It is found that the photocatalytic activity increased with the Ag_3VO_4 amount increasing, which can be ascribed to the matched energy structure in the Ag_3VO_4/β-$AgVO_3$ heterojunction that can efficiently enhanced separation of photoinduced carriers. The holes and hydroxyl radicals play significant roles in the photocatalytic degradation of RhB under visible light.

Acknowledgements

The authors would like to thank the partial financial support from the National Natural Science Foundation of China (No. 51272052 and No. 50902040).

Notes and references

1 M. R. Hoffmann, S. T. Martin, W. Choi and D. W. Bahnemann, *Chem. Rev.*, 1995, **95**, 69–96.
2 M. Zhang, C. C. Chen, W. H. Ma and J. C. Zhao, *Angew. Chem., Int. Ed.*, 2008, **47**, 9730–9733.
3 P. Zhou, J. G. Yu and M. Jaroniec, *Adv. Mater.*, 2014, **26**, 4920–4935.
4 R. A. Lucky and P. A. Charpentier, *Adv. Mater.*, 2008, **20**, 1755–1759.
5 L. Ge, M. X. Xu and H. B. Fang, *Mater. Lett.*, 2007, **61**, 63–66.
6 R. Asahi, T. Morikawa, T. Ohwaki, K. Aoki and Y. Taga, *Science*, 2001, **293**, 269–271.
7 J. G. Yu and X. X. Yu, *Environ. Sci. Technol.*, 2008, **42**, 4902–4907.
8 Y. Takahara, J. N. Kondo, T. Takata, D. Lu and K. Domen, *Chem. Mater.*, 2001, **13**, 1194–1199.
9 W. J. Chun, A. Ishikawa, H. Fujisawa, T. Takata, J. N. Kondo, M. Hara, M. Kawai, Y. Matsumoto and K. Domen, *J. Phys. Chem. B*, 2003, **107**, 1798–1803.
10 H. X. Li, Z. F. Bian, J. Zhu, D. Q. Zhang, G. S. Li, Y. N. Huo, H. Li and Y. F. Lu, *J. Am. Chem. Soc.*, 2007, **129**, 8406–8407.
11 L. Q. Ye, J. Y. Liu, C. Q. Gong, L. H. Tian, T. Y. Peng and L. Zan, *ACS Catal.*, 2012, **2**, 1677–1683.
12 J. X. Wang, H. Ruan, W. J. Li, D. Z. Li, Y. Hu, J. Chen, Y. Shao and Y. Zheng, *J. Phys. Chem. C*, 2012, **116**, 13935–13943.
13 C. L. Yu, G. Li, S. Kumar, K. Yang and R. C. Jin, *Adv. Mater.*, 2014, **26**, 892–898.
14 X. Yu, Z. H. Li, J. W. Liu and P. G. Hu, *Appl. Catal., B*, 2017, **205**, 271–280.
15 Q. Yuan, L. Chen, M. Xiong, J. He, S. L. Luo, C. T. Au and S. F. Yin, *Chem.–Eur. J.*, 2014, **255**, 394–402.
16 Q. X. Xiang, J. G. Yu and M. Jaroniec, *J. Phys. Chem. C*, 2011, **115**, 7355–7363.
17 P. Wang, B. B. Huang, X. Y. Qin, X. Y. Zhang, Y. Dai, J. Y. Wei and M. H. Whangbo, *Angew. Chem., Int. Ed.*, 2008, **47**, 7931–7933.
18 M. S. Zhu, P. L. Chen and M. H. Liu, *ACS Nano*, 2011, **6**, 4529–4536.
19 X. Lin, S. Y. Yu, Z. Y. Gao, X. X. Zhang and G. B. Che, *J. Mol. Catal. A: Chem.*, 2016, **411**, 40–47.
20 X. Lin, B. Wei, X. X. Zhang, M. S. Song, S. Y. Yu, Z. Y. Gao, H. J. Zhai, L. N. Zhao and G. B. Che, *Sep. Purif. Technol.*, 2016, **169**, 9–16.
21 Y. P. Bi, S. X. Ouyang, J. Y. Cao and J. H. Ye, *Phys. Chem. Chem. Phys.*, 2011, **13**, 10071–10075.
22 F. Guo, W. L. Shi, X. Lin, X. Yan, Y. Guo and G. B. Che, *Sep. Purif. Technol.*, 2015, **141**, 246–255.
23 X. Lin, X. Y. Guo, W. L. Shi, L. N. Zhao, Y. S. Yan and Q. W. Wang, *J. Alloys Compd.*, 2015, **635**, 256–264.
24 X. Lin, D. Xu, J. Zheng, M. S. Song, G. B. Che, Y. S. Wang, Y. Yang, C. Liu, L. N. Zhao and L. M. Chang, *J. Alloys Compd.*, 2016, **688**, 891–898.
25 X. Lin, Y. S. Wang, J. Zheng, C. Liu, Y. Yang and G. B. Che, *Dalton Trans.*, 2015, **44**, 19185–19193.
26 X. Lin, D. Xu, Y. Xi, R. Zhao, L. N. Zhao, M. S. Song, H. J. Zhai, G. B. Che and L. M. Chang, *Colloids Surf., A*, 2017, **513**, 117–124.
27 H. L. Lin, H. F. Ye, B. Y. Xu, J. Cao and S. F. Chen, *Catal. Commun.*, 2013, **37**, 55–59.
28 J. X. Wang, H. Ruan, W. J. Li, D. Z. Li, Y. Hu, J. Chen, Y. Shao and Y. Zheng, *J. Phys. Chem. C*, 2012, **116**, 13935–13943.
29 R. Ran, J. G. McEvoy and Z. S. Zhang, *Mater. Res. Bull.*, 2016, **74**, 140–150.
30 R. Ran, X. C. Meng and Z. S. Zhang, *Appl. Catal., B*, 2016, **196**, 1–15.
31 E. Akbarzadeh, S. R. Setayesh and M. R. Gholami, *RSC Adv.*, 2016, **6**, 14909–14915.
32 T. T. Zhu, Y. H. Song, H. Y. Ji, Y. G. Xu, Y. X. Song, J. X. Xia, S. Yin, Y. P. Li, H. Xu, Q. Zhang and H. M. Li, *Chem.–Eur. J.*, 2015, **271**, 96–105.
33 X. Lin, D. Xu, S. S. Jiang, F. Xie, M. S. Song, H. J. Zhai, L. N. Zhao, G. B. Che and L. M. Chang, *Catal. Commun.*, 2017, **89**, 96–99.
34 J. M. Song, Y. Z. Lin, H. B. Yao, F. J. Fan, X. G. Li and S. H. Yu, *ACS Nano*, 2009, **3**, 653–660.
35 H. S. Lin and P. A. Maggard, *Inorg. Chem.*, 2008, **47**, 8044–8052.
36 Z. Yi, J. Ye, N. Kikugawa, T. Kako, S. Ouyang, H. Stuart-Williams, H. Yang, J. Cao, W. Luo, Z. Li, Y. Liu and R. Withers, *Nat. Mater.*, 2010, **9**, 559–564.
37 P. Wang, B. B. Huang, X. Y. Zhang, X. Y. Qin, H. Jin, Y. Dai, Z. Y. Wang, J. Y. Wei, J. Zhan, S. Y. Wang, J. P. Wang and M. H. Whangbo, *Chem.–Eur. J.*, 2009, **15**, 1821–1824.
38 G. P. Dai, J. G. Yu and G. Liu, *J. Phys. Chem. C*, 2012, **116**, 15519–15524.
39 Y. M. Yang, Y. Y. Liu, B. B. Huang, R. Zhang, Y. Dai, X. Y. Qin and X. Y. Zhang, *RSC Adv.*, 2014, **4**, 20058–20061.
40 H. F. Shi, C. L. Zhang and C. P. Zhou, *RSC Adv.*, 2015, **5**, 50146–50154.
41 S. M. Wang, Y. Guan, L. P. Wang, W. Zhao, H. He, J. Xiao, S. G. Yang and C. Sun, *Appl. Catal., B*, 2015, **168**, 448–457.
42 H. D. Lu, J. X. Wang, Z. Y. Du, Y. P. Liu, M. Li, P. Chen and L. Z. Zhang, *Mater. Lett.*, 2015, **157**, 231–234.
43 X. Lin, X. Y. Guo, W. L. Shi, F. Guo, H. J. Zhai, Y. S. Yan and Q. W. Wang, *Catal. Commun.*, 2015, **66**, 67–72.
44 X. C. Shi and D. H. Wang, *Langmuir*, 2010, **26**, 9686–9694.
45 R. C. Oliveira, M. Assis, M. M. Teixeira, M. D. P. Silva, M. S. Li, J. Andres, L. Gracia and E. Longo, *J. Phys. Chem. C*, 2016, **120**, 12254–12264.
46 J. Zhao, C. Chen and W. Ma, *Top. Catal.*, 2005, **35**, 269–278.
47 X. K. Li and J. H. Ye, *J. Phys. Chem. C*, 2007, **111**, 13109–13116.
48 H. B. Fu, C. S. Pan, W. Q. Yao and Y. F. Zhu, *J. Phys. Chem. B*, 2005, **109**, 22432–22439.
49 H. M. Sung-Suh, J. R. Choi, H. J. Hah, S. M. Koo and Y. C. Bae, *J. Photochem. Photobiol., A*, 2004, **163**, 37–44.
50 A. Sari, C. Alkan and C. Bilgin, *Appl. Energy*, 2014, **136**, 217–227.